npj | computational materials

Article

Published in partnership with the Shanghai Institute of Ceramics of the Chinese Academy of Sciences

https://doi.org/10.1038/s41524-025-01943-5

Vacancy-controlled superconductivity in rock-salt carbides: towards predictive modelling of real-world superconductors

Simone Di Cataldo [1] ✉, William Cursio[1,2] & Lilia Boeri [1]

We critically reexamine the superconducting properties of rock-salt transition-metal carbides (TMCs), often regarded as textbook conventional superconductors, combining first-principles electron-phonon calculations with variable-composition evolutionary structure prediction. Studying superconducting trends across the entire transition-metal series, we find that, when the rock-salt stoichiometric phase is dynamically or thermodynamically unstable, carbon-vacant structures identified through unbiased structure prediction permit to reconcile theoretical calculations with experimental trends. Our integrated use of structure prediction and electron-phonon calculations defines a general framework for realistic modeling of superconductors shaped by non-equilibrium synthesis routes and defect tolerance.

Transition metal carbides (TMCs) are a broad class of materials formed by early transition metals and carbon, which crystallise in a rock-salt (NaCl-type) structure[1]. They serve as high-performance materials for cutting-tools, coatings, heat and chemical shields, due to their exceptional resistance. These carbides are metallic conductors ($\rho \sim 10^{-5}\Omega$m)[2] with high thermal conductivity[3]. When the transition metal (TM) belongs to groups V (V, Nb, Ta) and VI (Mo, W), TMCs also exhibit superconductivity, with critical temperatures (T_c) reaching up to 18 K in NbN-NbC-TiN alloys[4–9], and high critical fields[10].

So far, TMCs have found limited use in superconducting technologies due to their brittleness. However, there is a clear potential for applications as shock- and radiation-hard superconductors in extreme environments - such as cryogenic current leads on deep-space probes, kinetic-energy dampers, or compact fusion diagnostics - where the unparalleled hardness, erosion resistance, and thermal stability of TMCs could outweigh manufacturing challenges. Understanding in detail the relationships between crystal chemistry and superconducting properties is a crucial prerequisite to further optimize these materials and unlock their full technological potential.

To date, experimental data remains sparse and largely outdated, with most superconducting critical temperatures (T_c) reported in the 1960s and 1970s from samples synthesized at high temperatures. The data for TMCs with a finite T_c is summarized in Table 1, where we included, to the best of our knowledge, all experimental reports[5,8,9,11–27]. The table highlights a high variability in reported T_c's for elements in groups V and VI, which has been historically attributed to differences in carbon vacancy concentrations[14,15,17,28,29].

The microscopic understanding of superconductivity in TMCs is still superficial and fails to explain most experimental observations. In particular, although T_c is known to depend strongly on carbon content, existing studies on the role of vacancies are limited to the thermodynamic and mechanical stability of nonstoichiometric phases[30,31]. All first-principles studies of superconductivity so far have been based on the ideal 1:1 stoichiometric rock-salt structure, implicitly assuming its validity across the entire composition range. Recent work on group-IV and group-V compounds has interpreted variations in T_c in terms of the effect of electron filling of the transition-metal d states on the electron-phonon interaction[19,32,33], but failed to address the strong dependence of T_c on vacancy concentration highlighted in Table 1. TMCs containing group-VI elements were shown to be dynamically unstable in the 1:1 rock-salt structure, highlighting even further the limitations of describing these compounds in the stoichiometric phase[34,35].

In this work, we go beyond the 1:1 stoichiometric limit and systematically investigate the role of carbon vacancies on superconductivity across the TMC series, combining ab initio electron-phonon superconductivity theory and crystal structure prediction. Using unbiased evolutionary searches at variable compositions, we construct the TM-C phase diagrams, explicitly addressing the effect of non-stoichiometry. This leads us to identify a family of low-energy nonstoichiometric phases that preserve the rock-salt structure type, providing a natural explanation for the superconducting properties observed experimentally across the whole TMC series considered.

The main results across the whole TMC series are summarized by color-coding in Table 1. The TMs are ordered by the groups of the periodic

[1]Dipartimento di Fisica, Sapienza Università di Roma, Roma, Italy. [2]Leibniz Institute for Solid State and Materials Science Dresden (IFW Dresden), Dresden, Germany. ✉e-mail: simone.dicataldo@uniroma1.it

Table 1 | Summary of the thermodynamic and superconducting properties of various TMCs in the stoichiometric and vacant rock-salt structure

Comp.	Exp. T_c (K)	Dyn. st.	ΔH (meV/at.)	$N(E_F)$ (eV·sp.·at.)$^{-1}$	T_c^{McM} (K)	λ	ω_{log} (K)	Alt. Comp.	Dyn. st.	$N(E_F)$ (eV·sp.·at.)$^{-1}$	T_c^{McM} (K)	λ	ω_{log} (K)
ScC	< 1.4[11,12]	Y	106	0.36	5-10	0.6	461	Sc_6C_5	Y	0.37	2-5	0.5	417
YC	< 1.4	Y	356	0.41	10-14	0.8	364	Y_6C_5	Y	0.36	5-8	0.6	328
TiC	0–3.4[9,13]	Y	0	0.07	0-0	0.0	562	Ti_6C_5	Y	0.15	0-0	0.2	559
ZrC	< 0.3	Y	0	0.06	0-0	0.2	473	Zr_6C_5	Y	0.13	0-0	0.3	455
HfC	< 1.2	Y	0	0.07	0-0	0.2	427	Hf_6C_5	Y	0.12	0-0	0.3	394
VC	0–3.2[14]	Y	92	0.28	17-23	1.0	309	V_6C_5	Y	0.31	0-0	0.0	483
NbC	0–11.5[15,16,17,18,19,26]	Y	28	0.19	15-20	1.0	299	Nb_6C_5	Y	0.17	1-2	0.4	389
TaC	0–10.3[15,17,19,27]	Y	0	0.16	7-9	0.7	259	Ta_6C_5	Y	0.17	1-2	0.5	301
MoC	14.1[5,16,20,21,22,23]	N	288	0.33	-	-	-	Mo_6C_5	Y	0.32	18-21	1.4	209
WC	3.5–10[16,21]	N	420	0.28	-	-	-	W_6C_5	Y	0.16	5-8	0.7	239
ReC	3.4[24]	N	932	0.59	-	-	-	Re_6C_5	N	0.3	-	-	-

Green (red) cells highlight thermodynamical stability (instability) of the stoichiometric rock-salt phase. In red cells the calculated T_c for the stoichiometric phase is also in disagreement with experiment. ΔH, $N(E_F)$, T_C^{McM}, λ, and ω_{log} indicate the energy relative to the convex hull, the DOS at the Fermi energy, the calculated T_c, the *ep* coupling coefficient, and the average phonon frequency, respectively. Columns 1–8 indicate the properties of the stoichiometric (1:1) phase, while columns 9–14 indicate those of carbon-vacant (6:5) phase, for which the calculated and measured T_c values are in agreement. When available, direct references to experimental papers are given in the table. Other values are taken from refs. 8,9,25. The T_c's are computed using the McMillan formula[72,73], and the range is obtained using $\mu^* = 0.10$ and 0.15.

table, and colored in green when the stoichiometric phase is thermodynamically (meta)stable (within 50 meV/atom from the hull), and red otherwise. The table reports the main superconducting parameters for the stoichiometric (1:1) phase, and a carbon-vacant (6:5) phase which preserves the rock-salt geometry. We note that elements of group IV and V (Nb and Ta) are the only ones for which the stoichiometric phase is stable and here the calculated and measured values of T_c match. In groups III, VI and VII, the stoichiometric phase is instead unstable, and the calculated T_c's do not match experiments, while the carbon-vacant phase is found in much better agreement.

Our results demonstrate that thermodynamic stability is a crucial element in the realistic modeling of real-world superconductors[28,36].

Results and discussion

Thermodynamical properties

In Fig. 1, we show the ab-initio convex-hull diagrams calculated at ambient pressure for all TMCs in Table 1, using evolutionary algorithms for crystal structure prediction[37,38] (See the "Methods" section and the Supplementary Information for further details regarding DFT calculations, as well as additional figures detailing the electronic and structural properties).

The plots are arranged in order of increasing atomic numbers, from ScC to ReC. In these diagrams, each point indicates the formation energy of one specific structure, while the lines indicate the convex hull; points on the hull (blue circles) indicate structures thermodynamically stable against decomposition, whereas structures that lie above the hull are indicated as red squares. All computed convex hulls contain at least one stable composition; however, the depth varies systematically across the *d*-block: from about 1 eV/atom in group-IV compounds (TiC, ZrC, HfC) to around 0.1 eV in Mo-C, W-C and Re-C. As we will show, this trend mirrors the progressive filling of antibonding *d*-states, which are empty in group-IV TMCs, and the consequent weakening of the M-C bond[39]. The stoichiometric rock-salt phase is stable for elements of group IV and Ta (The 1:1 stoichiometry is stable in the MoC and WC system, but with a hexagonal structure, while the rock-salt geometry is high in energy, as shown in the diagram.). However, for elements in groups III, V, and VI, we also find a plethora of *sub-stoichiometric*, carbon-deficient phases—such as M_2C, M_3C_2, and M_6C_5—with rock-salt-like geometries (highlighted as green circles in Fig. 1). In several cases, these phases are more thermodynamically stable than the ideal 1:1 compound, or at least weakly metastable. While defects and vacancies typically increase the enthalpy and reduce the stability of a compound, our results point out that in rock-salt TMC they do the opposite.

In many cases, their powder diffraction patterns are nearly indistinguishable from that of the ideal 1:1 NaCl-type structure (see Supplementary Fig. 4). This suggests that many TMC samples for which finite critical temperatures were reported in past experiments may have actually contained nonstoichiometric, vacancy-rich phases rather than the nominal 1:1 compound. Indeed, this hypothesis is strongly supported by the fact that one such structure—M_6C_5— is an excellent model for capturing the effect of carbon vacancies in several TMCs. Before discussing superconducting properties, we first analyze general trends in thermodynamic stability, based on the calculated convex hulls.

Group III (Sc, Y): stable compositions include Y_2C and Y_4C_5; Sc_2C, Sc_4C_3, and Sc_3C_4, which have been experimentally reported[40–48]. All these the thermodynamically stable structures are qualitatively different from the NaCl structure, as they contain C_2, or C_3 chains.

The stoichiometric rock-salt structure is over 300 meV/atom above the convex hull. However, as the concentration of carbon vacancies increases, the relative energy of the rock-salt-like phases decreases drastically, to the point that the vacant rock-salt structure of Sc_2C (Y_2C) lies just 7 meV/atom (18 meV/atom) above the convex hull. These carbon-deficient phases may explain experimental reports of superconductivity in Sc and Y compounds nominally described as rock-salt carbides.

Experimental reports of a rock-salt ScC phase always involve a rapid quenching from extreme temperatures[11,12,46]. As for YC, although its T_c is cited in ref. 8, we were unable to retrieve the original source (ref. 49) to determine the synthesis conditions.

Group IV (Ti, Zr, Hf): the stoichiometric rock-salt structure is always thermodynamically stable. Carbon-vacant phases are present (Ti_6C_5, Ti_3C_2, Zr_6C_5, Hf_4C_3, Hf_3C_2), and their crystal structures retain a clearly recognizable rock-salt geometry throughout the 2:1 to 1:1 composition range. These results are in excellent agreement with the experimental report of synthesis of rocksalt structures with a wide range of vacancy concentrations[13,50]. In addition, for Zr we find on the convex hull a layered hexagonal phase with 2:1 composition, as also predicted in ref. 51, which has not been experimentally synthesized.

Group V (V, Nb, Ta): the stoichiometric rock-salt phase becomes progressively more stable down the group: the formation enthalpy is 92 meV/atom for V, 28 meV/atom for Nb, and negative for Ta. For all three

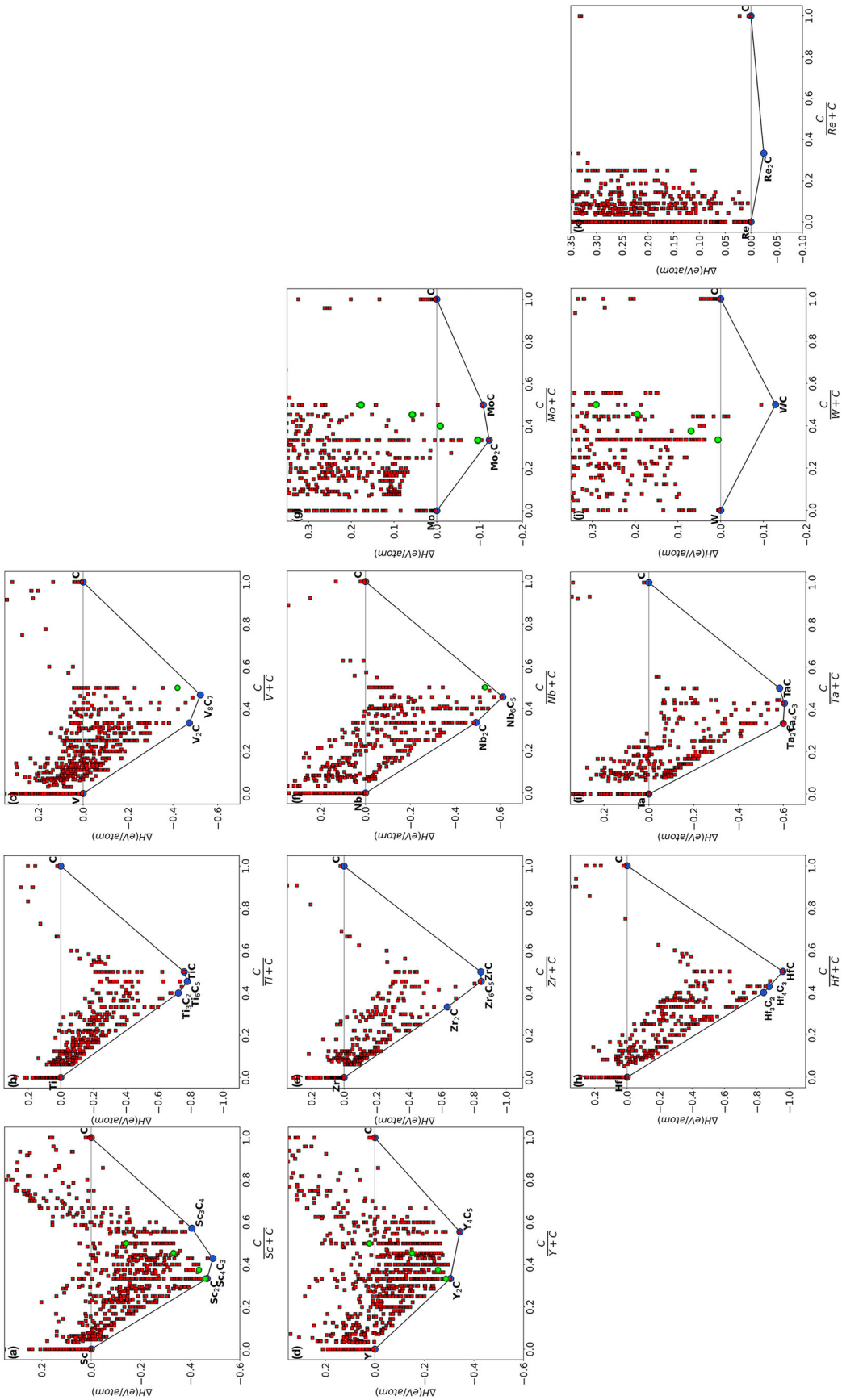

Fig. 1 | Convex hulls for TMC's at ambient pressure. The figures are ordered with increasing atomic number, and follow the disposition of the respective TMs in the periodic table. Thermodynamically stable and unstable structures that lie on/above the hull are indicated with blue circles and red squares, respectively. Metastable rock-salt structures with carbon vacancies are marked as green circles when above the convex hull.

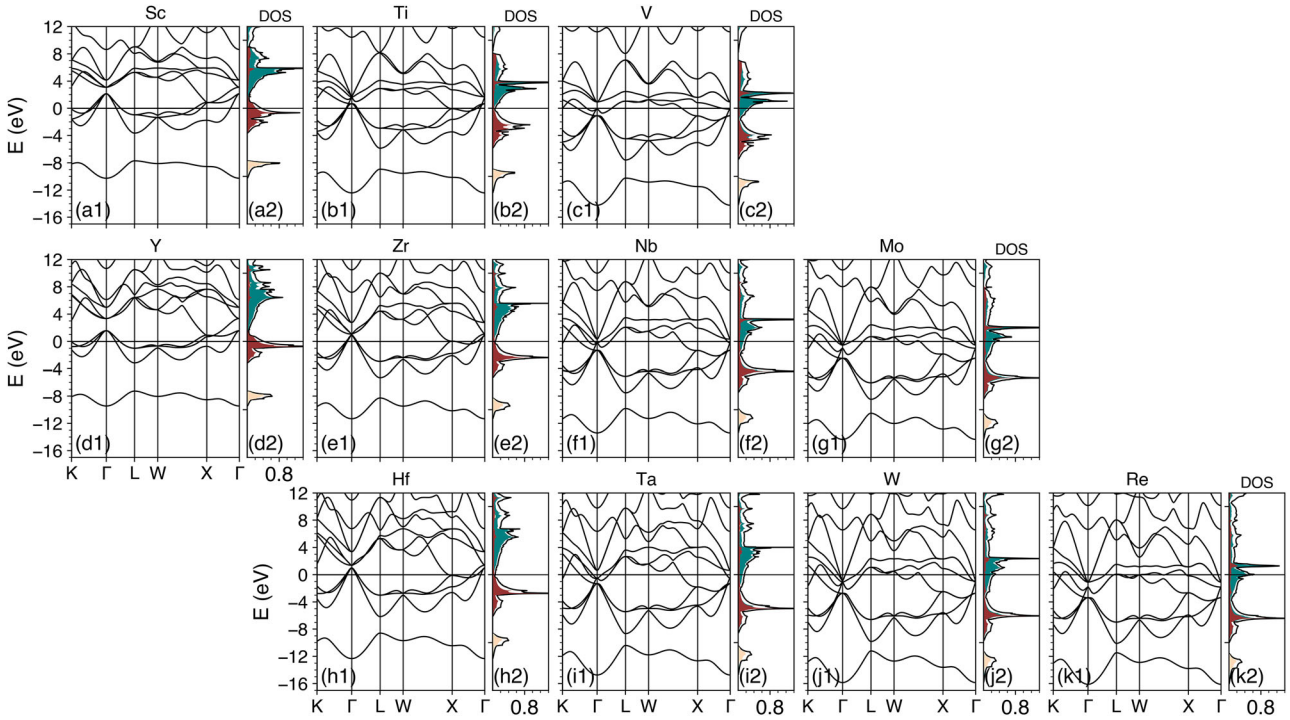

Fig. 2 | Electronic structure of TMC's at ambient pressure. Electronic band structures (left panels) and projected densities of states (right panels) for rock-salt MC (M = Sc-Re), ordered with increasing atomic number, and following the disposition of the respective TMs in the periodic table. Colour code: C-2*s* (orange), C-2*p* (dark red) and M-*d* (teal). The Fermi level is at $E = 0$. The DOS is in units of states/eV/spin/atom.

elements, we also find stable carbon-deficient rock-salt phases (V_8C_7, Nb_6C_5, Ta_4C_3) which, in the case of Nb and V, are more stable than the stoichiometric phase.

The presence of vacancies in group-V TMCs has been widely documented experimentally[52–56]. Some authors suggested the formation of vacancy superstructures[57–59] for both vanadium (V_6C_5[60,61] and V_8C_7[52,53]) and niobium (Nb_6C_5[17,54]). These observations strongly support our thermodynamic analysis.

Group VI (Mo, W): the stoichiometric rock-salt phase has a very high formation energy of 288 meV/atom (420 meV/atom) for Mo (W), making it strongly unstable. The thermodynamically stable phase for the 1:1 composition is, in fact, a hexagonal phase for both Mo and W, as confirmed by experiments[62]. We also found a 1:2 hexagonal phase on that is on the convex hull for Mo and very close for W[63–66].

Introducing vacancies in the rock-salt phase lattice lowers its relative formation energy dramatically, down to 26 meV/atom in Mo_2C (green circles in Fig. 1). Indeed, the experimental synthesis of the rock-salt phase through high-temperature melting and extreme quenching was reported for both MoC and WC[4,7,21]. This resulted in an intermediate, metastable phase stabilized by a certain amount of carbon vacancies[67].

Group VII (Re) In rhenium carbide the 1:1 rock-salt phase is 932 meV/atom above the hull, and even carbon vacancies are not enough to stabilize the lattice, with Re_6C_5 lying 688 meV/atom above the hull. Recent experiments also failed to reproduce a rock-salt phase[68]. We observe instead that ref. 24, which reports a rock-salt phase of ReC, reports a lattice parameter of 4.0 Å. This value is much closer to the calculated equilibrium lattice constant of Re (3.9) than that of ReC (4.4), suggesting that the samples of ref.[24] may have contained mostly pure Re, and, possibly, a small concentration of C impurities.

In summary, our results indicate that rock-salt-like TMC phases can be synthesized for a wide range of transition metals, even in cases where the 1:1 rock-salt structure is thermodynamically or dynamically unstable. Carbon vacancies play a key role in stabilizing these structures, lowering their formation energies and making them accessible as metastable phases.

This is reflected in the synthesis conditions reported in the literature: rock-salt-like phases are typically obtained via rapid quenching from the high-temperature melt[16,69]. Non-equilibrium synthesis methods are consistent with their metastable nature and the presence of a high vacancy concentration. Note that C-vacancies may not be always easy to detect through X-Ray Diffraction analysis, especially if they do not form an ordered superstructure.

Electronic structure

Figure 2 shows the electronic band structures and projected densities of states (DOS) of the eleven stoichiometric rock-salt carbides, arranged in the same order as the corresponding metals appear in the periodic table. For each TMC the left panel shows the electronic bands, while the right panel displays the DOS decomposed into C-2*s* (dark red), C-2*p* (orange), and M-*d* (teal) contributions.

The band structures of all compounds comprise the same three groups of bands: (i) a nearly flat, purely C-2*s* band between −9 and −8 eV; (ii) a broad ~10-eV-wide manifold around the Fermi level, which consists of six bands; (iii) weakly dispersive, metal-dominated states above.

The DOS corresponding to the broad manifold around the Fermi level exhibits a characteristic symmetric double feature: a sharp van-Hove peak with C-2*p* character, which declines towards a pseudo-gap, followed by a rise into another peak, with M-*d* character. These six bands derive from the hybridization of the three $d_{t_{2g}}$ orbitals of the M atom with the three C-*p* orbitals, and are clearly split into three *bonding* and three *antibonding* states, separated by a pseudogap.

The hybrid C-*p*/M-*d* manifold behaves in a rigid-band fashion across the TM series from group III to VII. For ScC and YC the Fermi level sits on the shoulder of the C-2*p* peak, resulting in a moderate DOS at the Fermi level (listed in Table 1). In TiC, ZrC and HfC E_F lines up almost exactly with the pseudogap. For these elements, the TM-C bond strength is maximum, because the tetravalent M atoms match the preferred carbon valence.

When, in group V (V, Nb, Ta) TMCs, an additional *d* electron is added, E_F is pushed onto the metal-dominated DOS peak above the gap. Finally, in

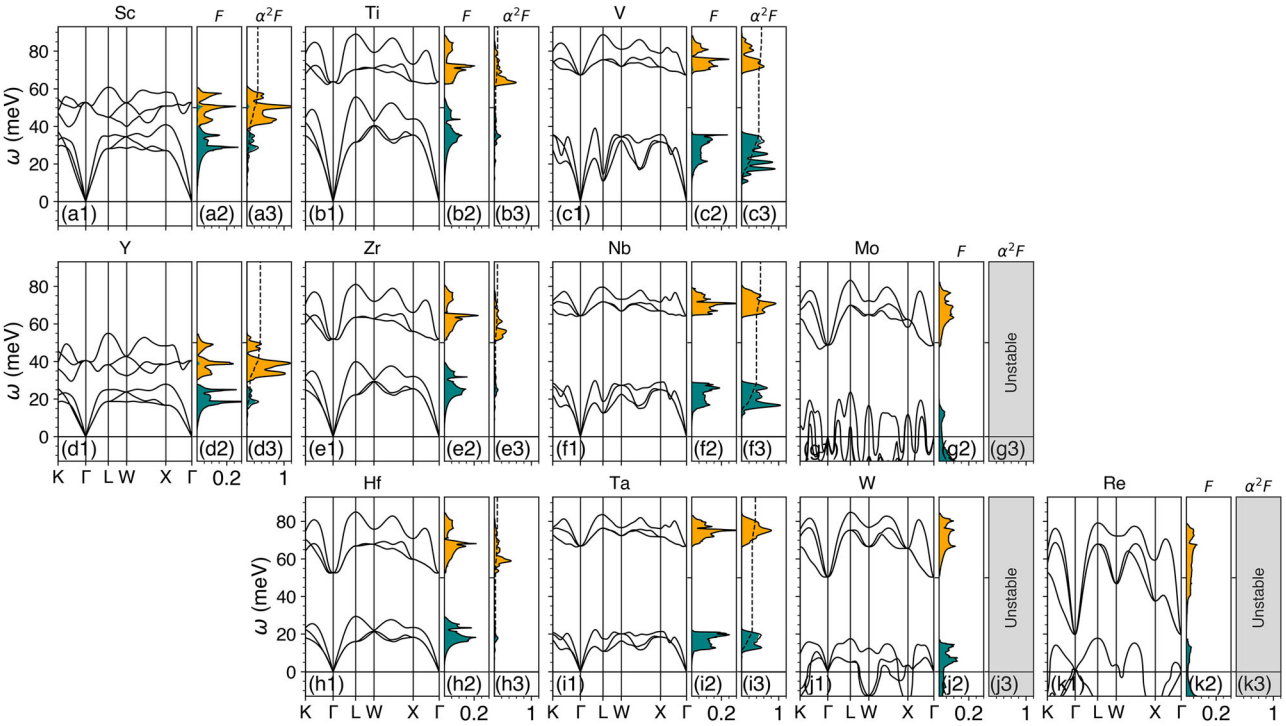

Fig. 3 | Phonon and electron-phonon properties of TMC's. Phonon dispersions, phonon DOS $F(\omega)$ and Eliashberg function $\alpha^2F(\omega)$ for rock-salt MC (M = Sc-Re). Orange (teal) shading indicates the projection onto carbon (transition metal) modes. The dashed line in the rightmost panel is the cumulative integral $\lambda(\omega)$. Grey panels mark dynamically unstable phases, for which we did not compute the electron-phonon properties.

Mo, W and Re (group VI), the Fermi level moves closer to the van-Hove singularity, so the DOS is even larger. However, as we shall see, this causes a dynamical instability of the stoichiometric rock-salt phase.

Moving down a group (e.g., Ti → Zr → Hf) mainly reduces the bandwidth, since TM with a larger atomic radius form TMCs with larger lattice parameters. This effect is particularly relevant in group V, where the theoretical equilibrium lattice parameter of Nb and Ta is almost identical (4.47 and 4.48 Å, respectively), but is significantly larger than that of V (4.15 Å). As a result, the DOS of V exhibits significantly sharper features; in particular, the value at E_F is 50% larger, resulting in a significantly larger T_c predicted for the stoichiometric 1:1 phase. (See Supplementary Table III for the list of calculated lattice parameters.

The thermodynamic stability indeed reflects quite closely the filling of the t_{2g}-C states: in group IV, where all bonding states are full, the depth of the hull is largest; in groups V–VII, as antibonding states are gradually filled, the 1:1 structure becomes first gradually less stable, and finally unstable in Mo, W and Re.

Lattice dynamics and electron-phonon coupling

We computed the phonon and superconducting properties of the TMC series using Density Functional Perturbation Theory[70,71] (See the "Methods" section for further details) in the stoichiometric rock-salt phase for all elements. The crystal structures, as well as further computational details are reported in the Supplementary Information.

Figure 3 presents the phonon dispersion along the same high-symmetry directions used for the electronic bands, together with the total and atom-projected phonon DOS $F(\omega)$ and the Eliashberg function $\alpha^2F(\omega)$. The panels for different TMCs are arranged in the same order as Fig. 1; the color code indicates the projection of the eigenmodes on carbon (orange) and transition-metal (teal) vibrations. The dashed curve in the rightmost panels indicates the frequency-dependent electron-phonon coupling constant $\lambda(\omega) = 2\int_0^\omega \alpha^2F(\Omega)/\Omega\, d\Omega$.

All spectra exhibit a gap between modes with mainly TM character, below 30 meV, and modes with dominant carbon character, at higher frequencies; the extent of the spectrum depends on the nature of the TM mode, and range from 60 meV in ScC and YC to 85 meV in all other cases. C-based vibrations are softer in TMCs containing group III elements because the incomplete filling of the corresponding bonding bands weakens the TMt_{2g}-C bonds. The dispersions of compounds containing group-IV and group-V elements are quite similar, although a pronounced softening is clearly seen along the W-X path. In TMCs containing groups VI and VII elements entire branches become imaginary: the stoichiometric MoC, WC and ReC structures are dynamically unstable. This is consistent both with their high formation energies and with the calculated electronic structure. In all three compounds, the Fermi level is very close to a van-Hove peak in the Density of States, which generally points to an instability towards a lower-symmetry structure with a lower DOS.

The variation in the relative shape of the phonon density of states - $F(\omega)$ - and electron-phonon spectral function - $\alpha^2F(\omega)$ - reveal marked differences in the nature of the electron-phonon coupling across the series. These differences reflect the same rigid-band trend observed in the electronic structure. In group III TMCs, where electronic states at the Fermi level have essentially C-p character, 75% of the total λ is concentrated in carbon vibrations. In group IV TMCs, where E_F lies in a pseudo-gap of the electronic DOS, the electron-phonon coupling is essentially zero; in group V TMCs, where the electronic DOS at E_F is dominated by TM $d_{t_{2g}}$ states, 75% of the total λ is due to TM vibrations.

Overall, the lattice dynamics and the nature of the electron-phonon coupling across the TMC series can be understood in terms of the filling of the metal t_{2g}-carbon bonding/antibonding manifold:

- in group III, partial filling of bonding states leads to soft phonons and strong coupling via carbon vibrations;
- in group IV, full bonding-state filling results in stiff lattices and negligible coupling due to the presence of a pseudogap at E_F;
- in group V, progressive filling of antibonding states enhances coupling through metal vibrations;
- in groups VI and VII, further filling of the antibonding states ultimately drives dynamical instabilities.

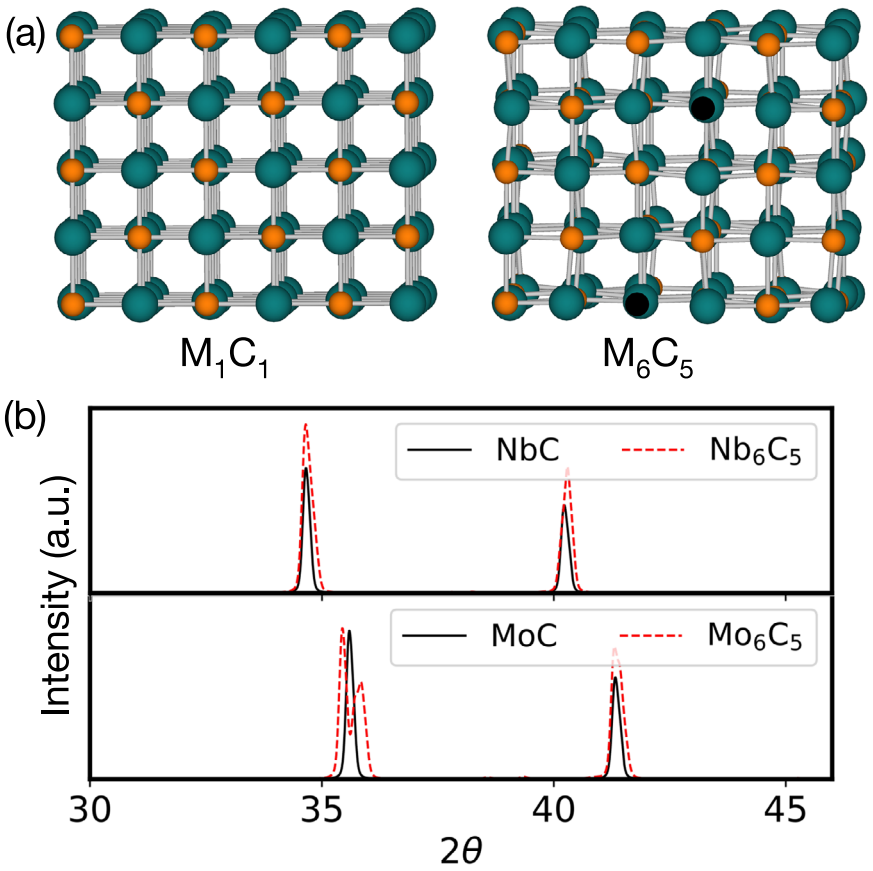

Fig. 4 | Comparison of the structures of stoichiometric (M_1C_1) and carbon-vacant (M_6C_5) TMCs. **a** The TM, C, and vacancies are indicated as large green, small orange, and small black spheres, respectively. **b** Simulated X-Ray powder diffraction pattern for stoichiometric (black line) and carbon-vacant (red line) MoC and NbC assuming a Cu K-α wavelength of 1.54059 Å. The pattern was convolved with a Gaussian width of 0.05 °.

Superconductivity

Using the calculated $\alpha^2F(\omega)$ we computed the superconducting T_c using the McMillan formula[72,73] (See Eq. (1)), with a a constant value of μ^* of 0.15.

The results are summarized in columns 5–8 of Table 1. The T_c calculated for the 1:1 stoichiometric rock-salt phase is within 30% of the experimental value for only five (Ti, Zr, Nb, Hf, Ta), out of the eleven elements studied, highlighted in green. For the remaining six, the T_c is either largely overestimated (Sc, V, Y), or could not be computed (Mo, W, Re), as the structure is dynamically unstable.

These discrepancies can be understood by analyzing not only the T_c, but considering also the enthalpy relative to the hull (ΔH). In all cases for which the predicted T_c for the stoichiometric rock-salt phase does not agree with experiment, the formation enthalpy is higher than 50 meV/atom, which is usually considered a practical threshold for metastability; moreover, in Mo, W, and Re, the rock-salt structure is even dynamically unstable. In other words, the disagreement does not indicate a limitation of conventional Migdal–Eliashberg theory; rather, it reflects the fact that quantitative predictions of T_c become unreliable when based on an incorrect structural model, instead of the true thermodynamic ground-state.

In fact, our analysis raises a crucial point: if the structure if the measured T_c does not correspond to the stoichiometric phase—and the calculated values confirm it—then what structure is actually measured in the experiments?

In the previous section, we have shown that carbon-vacant rock-salt-like structures lie on or close to the convex hull across the whole TMC series. In particular, in groups III, V, and VII, they are much more stable than the 1:1 phase. The most plausible explanation is that experiments were performed on such carbon-vacant phases, but the resolution of the powder diffraction spectra was not sufficient to resolve the concentration of carbon vacancies. For reference, in Fig. 4b, we compare the simulated X-Ray powder diffraction pattern for stoichiometric and vacant MoC and NbC. The main structure of the peaks is similar in both cases. In Mo, the main peak at 36° splits more evidently, while in Nb the vacancy-induced distortion requires a resolution of the order of 0.01-0.02° to be detected.

Carbon-vacant phases

To test this hypothesis, we computed the superconducting T_c for a carbon-vacant rock-salt structure with M_6C_5 composition ($M_1C_{0.83}$), represented in a reduced monoclinic cell (Structural information is given in the Supplementary Information). A visual comparison of the two structures is shown in Fig. 4. This structure corresponds to the experimentally observed crystal structure of Nb_6C_5[74], and was also independently reproduced by our unbiased crystal structure prediction calculations, which systematically placed it on or close to the convex hull across several TMCs. We selected it as a general, representative example of carbon-deficient rock-salt-like phases. The specific choice was motivated by the relatively small and symmetric unit cell, which makes *ep* calculations affordable, and by the weak vacancy-vacancy interactions expected for this geometry[30]. Comparing the stoichiometric and carbon-vacant phases, we see that all elements except W and Re undergo an expansion in the octahedral directions around the vacancy, i.e., the M atoms neighboring the vacancy are pushed away from it. In W and Re, the opposite trend occurs. For further details on this aspect, we refer the reader to Supplementary Figs. 2 and 3.

The calculated T_c's, reported in the 12th column of Table 1, are in significantly closer agreement with experiments for all elements that were not already described by the stoichiometric phase, except for rhenium. The comparison between the stoichiometric and carbon-vacant phase reveals two main effects: (i) in TMCs containing elements of group III and V, carbon vacancies suppress the T_c drastically. In group V, this suppression—combined with the presence of several weakly metastable vacancy-rich phases—naturally explains the broad spread of experimental T_c values; (ii) in group VI compounds, the carbon-vacant structure is dynamically stable, unlike the stoichiometric phase, and the calculated T_c's – around 18 K for Mo_6C_5, and 5 for W_6C_5—are in good agreement with the reported

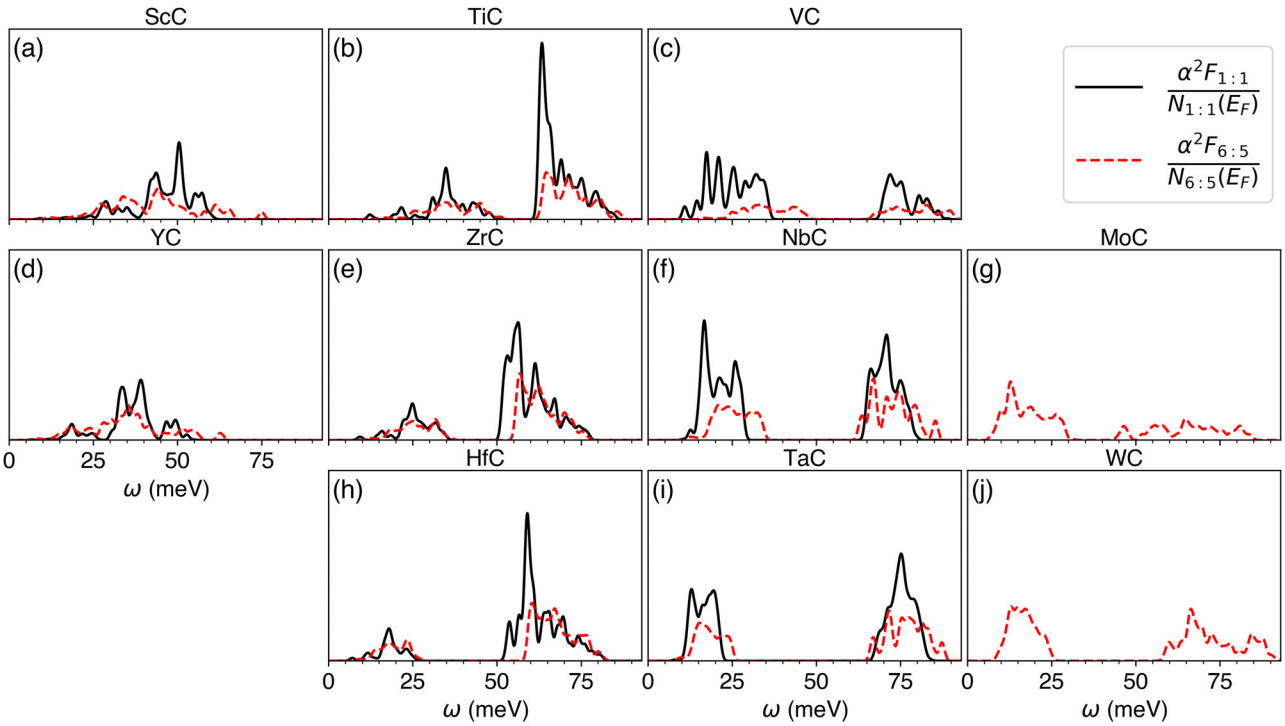

Fig. 5 | Electron-phonon properties of the stoichiometric and carbon-vacant phases. Comparison of the Eliashberg function ($\alpha^2F(\omega)$) for transition-metal carbides in the rock-salt stoichiometric phase (1:1, black, solid lines) and in the vacant M_6C_5 phase (6:5, red, dashed lines), rescaled by the electronic DOS at the Fermi energy, across the 3d, 4d, and 5d series.

experimental values. In contrast, Re_6C_5 is unstable, and no amount of vacancies can stabilize it. It is therefore likely that the T_c measured in ref. 24 originated from pure Re, or some other impurity in the sample.

For group V TMC, the experimental dependence on T_c on vacancy concentration has been investigated in detail. For VC, the nominal concentration is usually $VC_{0.88}$, which is not superconducting. Superconductivity can be induced by carbon implantation[14], reaching a maximum T_c of 3.2 K. In NbC, the dependence of T_c on C-vacancy concentration has been studied systematically. The rock-salt phase exhibits a maximum T_c of 11.1 K[9,16], but superconductivity is strongly suppressed as the number of vacancies is increased[15,17,75], vanishing completely for concentrations below $x = 0.77$. Tantalum behaves in a similar way, with a maximum T_c of 10.3 K[9], and a sharp decrease with carbon vacancies[15,17].

These observations naturally raise the question: why do carbon vacancies suppress superconductivity so strongly in group V TMCs?

The T_c of a superconductor can be written in terms of the McMillan formula[72]

$$T_c = \frac{\omega_{\log}}{1.20} \exp\left[-\frac{1.04(1+\lambda)}{\lambda - \mu^*(1+0.62\,\lambda)}\right] \quad (1)$$

Where λ, ω_{log}, and μ^* are the *ep* coupling constant, the logarithmic average phonon frequency, and the Morel–Anderson pseudopotential, respectively. The *ep* coupling constant can be approximated by Hopfield's expression

$$\lambda = \frac{N(E_F)\,\langle g^2\rangle}{M\langle\omega^2\rangle}, \quad (2)$$

A decrease in the superconducting T_c is most commonly associated to a decrease in λ which, in turn, can originate either from a decrease of $N(E_F)$, $\langle g^2\rangle$, or both.

The suppression of $N(E_F)$ is a well-established mechanism, which is often invoked to explain the suppression of T_c due to crystal imperfections, as some of us have recently shown in NbTi[76].

However, this mechanism does not apply to TMCs, as $N(E_F)$ remains essentially unchanged with vacancy concentration in group III and V TMC, while T_c is strongly suppressed – see columns 5-6 and 11-12 of Table 1 (We refer the reader to Supplementary Fig. 1 for the full DOS's).

Hence, the suppression of T_c must originate from a reduction of the *ep* matrix elements. To isolate this effect in Fig. 5, we compare the Eliashberg spectral functions of the stoichiometric and carbon-vacant phases, scaled by their respective $N(E_F)$ values. This scaling removes the trivial effect of the DOS in Hopfield's formula—Eq. (2)—so that any remaining discrepancy reflects a genuine change in the electron-phonon interaction strength and spectral distribution.

Figure 5 shows that in the TMCs of group V the suppression of coupling due to the introduction of carbon vacancies is particularly strong, and is accompanied by a sizable renormalization of the spectrum towards higher frequencies.

In this work, we reassessed superconductivity in rock-salt transition-metal carbides by combining first-principles electron-phonon calculations with variable-composition evolutionary structure prediction. Despite decades of study and the potential relevance of these compounds for rugged-environment superconductivity applications, a consistent microscopic description is still lacking. Our electron-phonon calculations show that the commonly assumed 1:1 stoichiometric rock-salt structure fails to reproduce experimental trends in T_c and is often dynamically or thermodynamically unstable. However, theory and experiment can be reconciled by properly accounting for carbon vacancies. In fact, unbiased evolutionary structure prediction identifies a family of low-energy, rock-salt-like nonstoichiometric phases that are both thermodynamically stable and consistent with the observed superconducting properties. The effect of carbon vacancies on T_c is highly nontrivial and can only be captured by structurally accurate models.

Our results definitively establish thermodynamic stability as a key factor for the modeling of real-world superconductors. Most large-scale technological applications rely on low-temperature superconductors synthesized under strongly non-equilibrium conditions, where defects, disorder, and synthesis history play a central role—yet are typically neglected in

state-of-the-art computational techniques. By integrating realistic structural thermodynamics into first-principles calculations, our approach sets a practical foundation for predictive modeling of superconductors under realistic synthesis conditions.

Methods

Computational details

Evolutionary crystal structure prediction calculations were performed with the Universal Structure Predictor: Evolutionary Xstallography (USPEX) code [37,38] using variable-composition sampling. The local relaxations were performed in a five-step procedure with progressively tighter constraints using VASP[77–79]. We employed projector-augmented wave pseudopotentials, and the Perdew-Burke-Ernzerhof (PBE) exchange-correlation functional, a plane-wave cut-off gradually raised from the recommended minimum up to 500 eV, Gaussian smearing down to 0.02 eV, and a k-point density down to 0.35 $Å^{-1}$.

All electronic, vibrational and superconducting properties were computed with QUANTUM ESPRESSO 7.3.1[70,71], after re-optimizing the structures. Optimized norm-conserving Vanderbilt PBE pseudopotentials[80] were adopted with a 100 Ry cut-off on the plane-wave expansion. A Methfessel–Paxton smearing of 0.02 Ry was used for charge-density integration, and a Gaussian smearing of 0.015 Ry for electron-phonon coupling integration.

Harmonic force constants were obtained within density-functional perturbation theory and Fourier-interpolated to obtain phonon DOS and dispersions.

Critical temperatures were obtained from the McMillan–Allen–Dynes formula using the calculated λ and $\omega_{\log}$ and a Coulomb pseudopotential $\mu^* = 0.10-0.15$. This choice is consistent with experimental determinations in classical superconductors and modern RPA-based ab-initio estimates for transition-metal systems[81–84].

Further details are available in the Supplementary Information.

Data availability

Data is provided within the manuscript or supplementary information files. CIF files for thermodynamically stable and other phases relevant for this study have been deposited through figshare and are accessible at the following https://doi.org/10.6084/m9.figshare.30156193.

Received: 9 June 2025; Accepted: 16 December 2025;
Published online: 04 February 2026

References

1. Williams, W. S. Transition-metal carbides. *Prog. Solid State Chem.* **6**, 57–118 (1971).
2. Modine, F., Foegelle, M., Finch, C. & Allison, C. Electrical properties of transition-metal carbides of group IV. *Phys. Rev. B* **40**, 9558 (1989).
3. Radosevich, L. & WILLIAMS, W. S. Thermal conductivity of transition metal carbides. *J. Am. Ceram. Soc.* **53**, 30–33 (1970).
4. Toth, L., Rudy, E., Johnston, J. & Parker, E. Superconducting critical temperatures of the carbides and nitrides with the NaCl structure: superconductivity of MOC. *J. Phys. Chem. Solids* **26**, 517–522 (1965).
5. Toth, L. & Zbasnik, J. Low temperature heat capacities of superconducting molybdenum carbides. *Acta Metall.* **16**, 1177–1182 (1968).
6. Pessall, N., Gold, R. & Johansen, H. A study of superconductivity in interstitial compounds. *J. Phys. Chem. Solids* **29**, 19–38 (1968).
7. Morton, N. et al. Superconductivity of molybdenum and tungsten carbides. *J. Less Common Met.* **25**, 97–106 (1971).
8. Vonsovsky, S. V., Izyumov, Y. A., Kurmaev, E., Brandt, E. & Zavarnitsyn, A. *Superconductivity of Transition Metals: Their Alloys and Compounds*, Vol. 27 (Springer, 1982).
9. Toth, L. *Transition Metal Carbides and Nitrides* (Elsevier, 2014).
10. Fink, H., Thorsen, A., Parker, E., Zackay, V. F. & Toth, L. High-field superconductivity of carbides. *Phys. Rev.* **138**, A1170 (1965).
11. Nowotny, H. & Auer-Welsbach, H. Über das scandiumcarbid. *Monatshefte für Chemie und Verwandte Teile anderer Wissenschaften* **92**, 789–793 (1961).
12. Samsonov, G. V., Makarenko, G. & Kosolapova, T. Y. Scandium carbides and compound scandium-titanium carbides. In *Doklady Akad. Nauk SSSR*, Vol. 144 (Inst. of Metal-Ceramics and of Special Alloys, Academy of Sciences, USSR, 1962).
13. Klimashin, G., Neshpor, V., Nikitin, V., Novikov, V. & Shalyt, S. *Superconductivity of Titanium Carbide*. (Technical Report, Semiconductor Institute, Moscow, 1970).
14. Geerk, J., Langguth, K., Linker, G. & Meyer, O. The influence of implanted ions on the superconducting transition temperature of transition metals and transition metal carbides. *IEEE Trans. Magn.* **13**, 662–665 (1977).
15. Giorgi, A., Szklarz, E., Storms, E., Bowman, A. L. & Matthias, B. Effect of composition on the superconducting transition temperature of tantalum carbide and niobium carbide. *Phys. Rev.* **125**, 837 (1962).
16. Willens, R., Buehler, E. & Matthias, B. Superconductivity of the transition-metal carbides. *Phys. Rev.* **159**, 327 (1967).
17. Toth, L., Ishikawa, M. & Chang, Y. Low temperature heat capacities of superconducting niobium and tantalum carbides. *Acta Metall.* **16**, 1183–1187 (1968).
18. Yan, D. et al. Superconductivity and fermi-surface nesting in the candidate Dirac semimetal NBC. *Phys. Rev. B* **102**, 205117 (2020).
19. Shang, T. et al. Superconductivity and topological aspects of the rocksalt carbides nbc and tac. *Phys. Rev. B* **101**, 214518 (2020).
20. Clougherty, E., Lothrop, K. & Kafalas, J. A new phase formed by high-pressure treatment: face-centred cubic molybdenum monocarbide. *Nature* **191**, 1194–1194 (1961).
21. Willens, R. H. & Buehler, E. The superconductivity of the monocarbides of tungsten and molybdenum. *Appl. Phys. Lett.* **7**, 25–26 (1965).
22. Sadagapan, V. & Gatos, H. Superconductivity in the transition metal carbides: Mo4. 8si3c0. 6, mo0. 95hf0. 05c0. 75 and mo2c. *J. Phys. Chem. Solids* **27**, 235–238 (1966).
23. Sathish, C. et al. Superconducting and structural properties of δ-moc0. 681 cubic molybdenum carbide phase. *J. Solid State Chem.* **196**, 579–585 (2012).
24. Popova, S., Fomicheva, L. & Khvostantsev, L. Synthesis and superconductive properties of cubic rhenium monocarbide. *Zh. Ehksp. Teor. Fiz., Pis.' ma Red.* **16**, 609–610 (1972).
25. Matthias, B. T., Geballe, T. H. & Compton, V. B. Superconductivity. *Rev. Mod. Phys.* **35**, 1–22 (1963).
26. Zhang, D., Chen, C., Yan, D., Shi, Y. & Lu, X. Fully-gapped superconductivity in single crystalline nbc and tac probed by point-contact spectroscopy. *Supercond. Sci. Technol.* **35**, 125004 (2022).
27. Yan, D. Y. et al. Superconductivity in centrosymmetric topological superconductor candidate tac. *Supercond. Sci. Technol.* **34**, 035025 (2021).
28. Schwarz, K. & Rosch, N. Effects of carbon vacancies in nbc on superconductivity. *J. Phys. C Solid State Phys.* **9**, L433 (1976).
29. Pickett, W., Klein, B. & Zeller, R. Electronic structure of the carbon vacancy in nbc. *Phys. Rev. B* **34**, 2517 (1986).
30. Jang, J. H., Lee, C.-H., Heo, Y.-U. & Suh, D.-W. Stability of (ti, m) c (m= nb, v, mo and w) carbide in steels using first-principles calculations. *Acta Mater.* **60**, 208–217 (2012).
31. Muchiri, P., Korir, K., Makau, N. & Amolo, G. The impact of anionic vacancies on the mechanical properties of nbc and nbn: an ab initio study. *Comput. Mater. Sci.* **203**, 111113 (2022).
32. Noffsinger, J., Giustino, F., Louie, S. G. & Cohen, M. L. First-principles study of superconductivity and fermi-surface nesting in ultrahard transition metal carbides. *Phys. Rev. B Condens. Matter Mater. Phys.* **77**, 180507 (2008).

33. Sun, W., Ehteshami, H. & Korzhavyi, P. A. Structure and energy of point defects in tic: an ab initio study. *Phys. Rev. B* **91**, 134111 (2015).
34. Abrikosov, I., Vekilov, Y. K., Katsnelson, M. & Lichtenstein, A. Phonon related properties of transition metals, their carbides, and nitrides: a first-principles study. *J. Appl. Phys.* **101**, 123519 (2007).
35. Connétable, D. First-principles study of transition metal carbides. *Mater. Res. Express* **3**, 126502 (2016).
36. Klein, B., Papaconstantopoulos, D. & Boyer, L. Linear-combination-of-atomic-orbitals-coherent-potential-approximation studies of carbon vacancies in the substoichiometric refractory monocarbides nbc_x, tac_x, and hfc_x. *Phys. Rev. B* **22**, 1946 (1980).
37. Oganov, A. R. & Glass, C. W. Crystal structure prediction using ab initio evolutionary techniques: Principles and applications. *J. Chem. Phys.* **124**, 244704 (2006).
38. Lyakhov, A. O., Oganov, A. R., Stokes, H. T. & Zhu, Q. New developments in evolutionary structure prediction algorithm {USPEX}. *Comput. Phys. Commun.* **184**, 1172 – 1182 (2013).
39. Hugosson, H. W. et al. Theory of phase stabilities and bonding mechanisms in stoichiometric and substoichiometric molybdenum carbide. *J. Appl. Phys.* **86**, 3758–3767 (1999).
40. Giorgi, A., Szklarz, E., Krupka, M., Wallace, T. & Krikorian, N. Occurrence of superconductivity in yttrium dicarbide. *J. Less Common Met.* **14**, 247 (1968).
41. Atoji, M. & Kikuchi, M. Crystal structures of cubic and trigonal yttrium hypocarbides; a dimorphically interphased single-crystal study. *J. Chem. Phys.* **51**, 3863–3872 (1969).
42. Gschneidner, K. & Calderwood, F. The c- sc (carbon-scandium) system. *Bull. Alloy Phase Diagr.* **7**, 559–560 (1986).
43. Poettgen, R. & Jeitschko, W. Scandium carbide, sc3c4, a carbide with c3 units derived from propadiene. *Inorg. Chem.* **30**, 427–431 (1991).
44. Czekalla, R., Hüfken, T., Jeitschko, W., Hoffmann, R.-D. & Pöttgen, R. The rare earth carbidesr4c5withr= y, gd, tb, dy, and ho. *J. Solid State Chem.* **132**, 294–299 (1997).
45. Amano, G., Akutagawa, S., Muranaka, T., Zenitani, Y. & Akimitsu, J. Superconductivity at 18 k in yttrium sesquicarbide system, Y2C3. *J. Phys. Soc. Jpn.* **73**, 530–532 (2004).
46. Juarez-Arellano, E. A. et al. Formation of scandium carbides and scandium oxycarbide from the elements at high-(p, t) conditions. *J. Solid State Chem.* **183**, 975–983 (2010).
47. Juarez-Arellano, E. A. et al. In situ observation of the reaction of scandium and carbon by neutron diffraction. *J. Alloys Compd.* **509**, 1–5 (2011).
48. Aslandukova, A. et al. Novel high-pressure yttrium carbide γ-y 4 c 5 containing [c 2] and nonlinear [c 3] units with unusually large formal charges. *Phys. Rev. Lett.* **127**, 135501 (2021).
49. Samsonov, G., Makarenko, G. & Kosolapova, T. Y. Preparation and properties of yttrium monocarbide. *Zhur. Priklad. Khim.* **34**, 1444 (1961).
50. Goretzki, H. Neutron diffraction studies on titanium-carbon and zirconium-carbon alloys. *Phys. Status Solidi B* **20**, K141–K143 (1967).
51. Guo, Y. et al. Structural transitions and mechanical properties of Zr2C under ambient and high-pressure conditions. *Struct. Sci.* **78**, 848–856 (2022).
52. Henfrey, A. & Fender, B. A neutron diffraction investigation of v8c7. *Struct. Sci.* **26**, 1882–1883 (1970).
53. Wang, B., Liu, Y. & Ye, J. Mechanical properties and electronic structures of vc, v4c3 and v8c7 from first principles. *Phys. Scr.* **88**, 015301 (2013).
54. Landesman, J., Christensen, A., De Novion, C., Lorenzelli, N. & Convert, P. Order-disorder transition and structure of the ordered vacancy compound nb6c5: powder neutron diffraction studies. *J. Phys. C Solid State Phys.* **18**, 809 (1985).
55. Gao, X.-P., Jiang, Y.-H., Liu, Y.-Z., Zhou, R. & Feng, J. Stability and elastic properties of NbxCy compounds. *Chin. Phys. B* **23**, 097704 (2014).
56. Wu, L. et al. The phase stability and mechanical properties of Nb–C system: Using first-principles calculations and nano-indentation. *J. Alloys Compd.* **561**, 220–227 (2013).
57. Carlson, O., Ghaneya, A. & Smith, J. The c- v (carbon-vanadium) system. *Bull. Alloy Phase Diagr.* **6**, 115–124 (1985).
58. Smith, J., Carlson, O. & De Avillez, R. The niobium-carbon system. *J. Nucl. Mater.* **148**, 1–16 (1987).
59. Kostenko, M. & Rempel, A. Superimposure of m_6x_5 superstructures in ordered niobium carbide $nbc_{0.83}$. *Bull. Russian Acad. Sci.: Phys.* **82**, 595–599 (2018).
60. Venables, J., Kahn, D. & Lye, R. Structure of the ordered compound v6c5. *Philos. Mag.: A J. Theor. Exp. Appl. Phys.* **18**, 177–192 (1968).
61. Hiraga, K. Vacancy ordering in vanadium carbides based on v6c5. *Philos. Mag.* **27**, 1301–1312 (1973).
62. Schuster, J., Rudy, E. & Nowotny, H. The “moc”-phase with wc structure. *Monatshefte für Chemie/Chem. Mon.* **107**, 1167–1176 (1976).
63. Lautz, G. & Schneider, D. Über die Supraleitung in den Wolframkarbiden w2c und wc. *Z. für. Naturforsch. A* **16**, 1368–1372 (1961).
64. Parthé, E. & Sadogopan, V. The structure of dimolybdenum carbide by neutron diffraction technique. *Acta Crystallogr.* **16**, 202–205 (1963).
65. Giorgi, A. Superconductivity in the w-tc and w2c-tc systems. *Phys. B + C.* **135**, 420–422 (1985).
66. Page, K. et al. Reciprocal-space and real-space neutron investigation of nanostructured Mo2C and WC. *Solid State Sci.* **10**, 1499–1510 (2008).
67. Yvon, K., Nowotny, H. & Benesovsky, F. Zur Kristallstruktur von w 2 c: Kurze Mitteilung. *Monatshefte für. Chem.-Chem. Mon.* **99**, 726–729 (1968).
68. Juarez-Arellano, E. A. et al. Reaction of rhenium and carbon at high pressures and temperatures. *Z. für. Kristallographie-Crystalline Mater.* **223**, 492–501 (2008).
69. Nakamura, K. & Yashima, M. Crystal structure of nacl-type transition metal monocarbides mc (m= v, ti, nb, ta, hf, zr), a neutron powder diffraction study. *Mater. Sci. Eng. B* **148**, 69–72 (2008).
70. Giannozzi, P. Quantum espresso: a modular and open-source software project for quantum simulations of materials. *J. Phys. Condens. Matter* **21**, 395502 (2009).
71. Giannozzi, P. et al. Advanced capabilities for materials modelling with Quantum Espresso. *J. Phys. Condens. Matter* **29**, 465901 (2017).
72. McMillan, W. L. Transition Temperature of Strong-Coupled Superconductors. *Phys. Rev.* **167**, 331–344 (1968).
73. Allen, P. B. & Dynes, R. C. Transition temperature of strong-coupled superconductors reanalyzed. *Phys. Rev. B* **12**, 905–922 (1975).
74. Rempel, A. A., Gusev, A. I., Zubkov, V. & Shveikin, G. P. Structure of ordered niobium carbide nb_6c_5. *Soviet Phys. Doklady* **29**, 257 (1984).
75. Geerk, J. & Langguth, K.-G. Implantation and diffusion of carbon into niobium carbide single crystals. *Solid State Commun.* **23**, 83–87 (1977).
76. Cucciari, A., Naddeo, D., Di Cataldo, S. & Boeri, L. Nbti: a nontrivial puzzle for the conventional theory of superconductivity. *Phys. Rev. B* **110**, L140502 (2024).
77. Kresse, G. & Hafner, J. Ab initio. *Phys. Rev. B* **47**, 558–561 (1993).
78. Kresse, G. & Furthmüller, J. Efficient iterative schemes for ab initio total-energy calculations using a plane-wave basis set. *Phys. Rev. B* **54**, 11169–11186 (1996).
79. Kresse, G. & Joubert, D. From ultrasoft pseudopotentials to the projector augmented-wave method. *Phys. Rev. B* **59**, 1758–1775 (1999).
80. Hamann, D. R. Optimized norm-conserving Vanderbilt pseudopotentials. *Phys. Rev. B* **88**, 085117 (2013).
81. Shen, L. Tunneling into a high-t c superconductor-nb 3 sn. *Phys. Rev. Lett.* **29**, 1082 (1972).

82. Leavens, C. & Carbotte, J. An important parameter in high-temperature superconductivity. *J. Low. Temp. Phys.* **14**, 195–211 (1974).
83. Allen, P. B. & Mitrovic, B. Theory of superconducting Tc. *Solid State Phys.* **37**, 1–92 (1983).
84. Pellegrini, C., Kukkonen, C. & Sanna, A. Ab initio calculations of superconducting transition temperatures: When going beyond RPA is essential. *Phys. Rev. B* **108**, 064511 (2023).

Acknowledgements

L.B. and S.D.C. acknowledge computational resources from the EuroHPC project "EXCHESS" (EHPC-REG-2024R01-089) and funding from the European Union - NextGenerationEU under the Italian Ministry of University and Research (MUR), “Network 4 Energy Sustainable Transition - NEST” project (MIUR project code PE000021, Concession Degree No. 1561 of October 11, 2022) - CUP B53C22004070006. The authors thank Flavio Giuliani for useful discussion.

Author contributions

S.D.C. and L.B. conceived and initiated the project. W.C. carried out the phonon and electron-phonon calculations on cubic TMC. S.D.C. performed crystal structure prediction, and extended the analysis to carbon-vacant systems. L.B. supervised the research and secured funding, while S.D.C. acquired computational resources. S.D.C prepared all figures and tables. S.D.C. and L.B. drafted the manuscript with contributions from W.C. All authors reviewed, edited, and approved the final version.

Competing interests

The authors declare no competing interests.

Additional information

Supplementary information The online version contains supplementary material available at https://doi.org/10.1038/s41524-025-01943-5.

Correspondence and requests for materials should be addressed to Simone Di Cataldo.